Materials Science & Engineering A 785 (2020) 139364

Contents lists available at ScienceDirect

Materials Science & Engineering A

journal homepage: http://www.elsevier.com/locate/msea

Plastic deformation of pure copper in ultrasonic assisted micro-tensile test

Jiarui Kang [a], Xun Liu [a,*], Mingjie Xu [b]

[a] The Ohio State University, EJTC, 1248 Arthur Adams Drive, Columbus, OH, 43221, United States
[b] Irvine Materials Research Institute, University of California Irvine, Irvine, CA, 92697, United States

ARTICLE INFO

Keywords:
Power ultrasonics
Infrared imaging
Flow stress reduction
Digital image correlation
EBSD

ABSTRACT

The softening effect of ultrasonic vibration on pure copper is studied from a new perspective with micro-tensile tests, where the gauge length of the specimen is one order of magnitude smaller than the ultrasonic wavelength. With this configuration, the amount of flow stress reduction increases linearly with vibration amplitude whereas the flow stress reduction is insensitive to the studied strain rate ranging from 0.06/s to 1/s. Temperature rise associated with ultrasonic vibration is minimal from infrared thermal imaging. In situ digital image correlation (DIC) analysis shows strain localization near ultrasonic source whereas uniform strain distribution was observed during conventional tensile test. Optical microstructure characterization shows that area fraction of annealing twins in the deformed copper reduced from 3.3% to 1.8% with ultrasonic vibration. This is possibly attributed to enhanced interaction of dislocation between twin boundaries which act as non-regenerative dislocation source. Electron backscatter diffraction (EBSD) results show that ultrasonic vibration promotes preferential grain re-orientation and reduces the misorientation within grains.

1. Introduction

Early studies dating back from the 1950s by Blaha and Langenecker [1] show that the application of ultrasonic vibration significantly alters material behavior during plastic deformation. They observed an immediate reduction in flow stress when a high frequency vibration was applied and that the reduction of yield strength is generally invariant in the frequency range of 15–80 kHz [2]. They attributed this to the preferential absorption of acoustic energy at local dislocations and grain boundaries, which increases the mobility of dislocations and reduces the resistance to plastic deformation [3]. The ultrasonic softening effect has been successfully utilized in several metal forming processes such as wire drawing [4], extrusion [5], and incremental sheet forming [6], where a reduction of forming force was reported consistently.

Although the potential benefits of applying ultrasonic energy have been known for several decades and considerable amount of experimental and numerical analyses have been performed, the underlying physical principles remain elusive. There are mainly two groups of theories, namely stress superposition and direct acoustic softening. According to the theories of stress superposition, the plastic behavior of material remains unchanged under ultrasonic vibration and the softening effect is purely a result of macroscopic superposition of steady and alternating stress. The argument against local energy absorption of dislocation by resonance is based on the consideration that the applied ultrasonic frequency was orders of magnitude smaller than the natural frequency of a dislocation loop, which is in the range of 10^8 Hz. Gale [7] studied the effects of vibration on the yield strength of low carbon steel and found that the reduction of yield strength is invariant in the frequency range of 15–80 kHz and a temperature range of 30–500 °C, which is contrary to what a dislocation relaxation mechanism would suggests. The stress superposition theory can partially capture the drop of flow stress during the period of ultrasonic vibration. However, the total amount of reduction on the stress-strain curve is generally higher than the result of stress superposition [8]. Furthermore, the residual hardening or softening effect after ultrasonic vibration is stopped can hardly be explained. This indicates that microstructure of the material is modified under the ultrasonic treatment and accordingly the plastic deformation behavior is changed permanently. Dutta et al. [9] reported that ultrasonic vibration reduces the amount of dislocation density and restrains the formation of subgrain in BCC low carbon steel. They attributed the softening effect to the ultrasonically facilitated dislocation dipole annihilation and recovery. Siu et al. [10] also explained softening of FCC aluminum based on ultrasonically assisted recovery process but they observed enhanced subgrain formation. This on one hand is due to the different slip systems from FCC to BCC material. In addition, the ultrasonic vibration direction is perpendicular to the compression

* Corresponding author.
E-mail address: liu.7054@osu.edu (X. Liu).

https://doi.org/10.1016/j.msea.2020.139364
Received 21 January 2020; Received in revised form 2 April 2020; Accepted 3 April 2020
Available online 10 April 2020

direction in their experimental configuration. Zhou et al. [11] observed residual hardening for aluminum while residual softening for HCP α titanium. For aluminum, an increase of substructures, such as low angle grain boundaries and sub-grains leads to boundary strengthening and therefore residual hardening. For titanium, generation of deformation twinning is accelerated when ultrasonic vibration is applied. The twinning saturation is reached at a smaller plastic strain, after which the number of twinning is reduced with continued deformation. Liu et al. [12] observed similar microstructure change and residual softening phenomenon during ultrasonically assisted compression of pure titanium. Despite these debates among stress superposition and direct acoustic softening, it is nowadays more acceptable that the softening is contributed by both these two factors [2].

Several constitutive material models have been developed to describe the acoustic softening effect. Siddiq and Sayed [13] proposed a phenomenological crystal plasticity model with the assumption that the absorption of acoustic energy is highly localized at dislocations and grain boundaries. In their model, the plastic flow rule is modified so that the presence of acoustic energy decreases the critical resolved shear stress for each slip system. Sedaghat et al. [14] developed a constitutive model based on the thermal activation of dislocation gliding, where the acoustic energy is incorporated as a reduction of the activation energy. The plastic shear strain rate increases with higher amount of acoustic energy input into the system. Deshpande and Hsu [15] integrated ultrasonic effect into the dislocation density evolution model, where the increase in plastic shear strain rate results in the reduction of dislocation density.

So far in literature, ultrasonic assisted (UA) material tests fall into two categories: large-scale tension and small-scale compression, both of which have certain limitations. The initial UA tensile system from Blaha and Langenecker [1] that discovered acoustic softening has been adopted by several following studies [16–18], where the longitudinal length of the tensile specimen is tuned at either single or multiple halves of the ultrasound propagation wavelength in the corresponding material. Concerns with this configuration are that the vibration amplitude is non-uniformly distributed throughout the specimen. In addition, as the specimen is elongated during tensile loading, the initial resonant frequency becomes out of tuned. This potentially explains the scattered results reported in literature. The second group of UA tests focuses on small scale compression [19–21]. Although the above two issues with large scale tension can be eliminated, during compression, the associated frictional effects can hardly be decoupled from bulk acoustic softening. This interfacial frictional heat can cause additional thermal softening [12]. Additionally, in these literature reported experimental studies, strain is measured from the displacement of crosshead or through an extensometer [9], which only shows the overall change in length, and lacks detailed information of localized strain distribution to understand ultrasonic effects during plastic deformation.

In this work, ultrasonic assisted micro-tensile tests of pure copper were conducted, where the gauge length of the sample is in the millimeter scale and only 2.8% of the ultrasonic wavelength. Accordingly, change of amplitude of ultrasonic vibration along the sample is assumed to be small. To reveal the effects of ultrasound on strain distribution and deformation field during the tensile test, in situ digital image correlation analysis was performed.

2. Experiments

The ultrasonic assisted micro-tensile test frame was adapted from an apparatus originally developed for testing single crystal materials at The Ohio State University [22]. Schematic illustration and the actual setup are shown in Fig. 1 (a) and (b), respectively. The entire micro-tensile system is mounted onto a vibration cancellation table for isolating environmental disturbance. Dogbone sample is constrained within the grooves machined into the two tensile grips. One of the grips is stationary and directly connected to a magnetostrictive ultrasonic transducer, which can operate over a broad frequency range from DC to 20 kHz. The other grip is connected to a high spatial resolution linear actuator, in between which a whetstone bridge based load cell is installed to measure the dynamic tensile force during testing. The position of this moving grip is recorded using a capacitance displacement gauge, from which the engineering strain of the specimen can be calculated. In order to accurately reveal the detailed strain distribution, a high speed camera is mounted on top of the sample for in situ imaging of deformation, slip band formation and crack initiation. The images are post processed with Ncorr [23], a 2D digital image correlation (DIC) analysis program, to obtain the full-field displacement and true strain evolution during tensile tests. Micron-scale speckled pattern are prepared on specimen surface prior to tests by sprinkling printer toner on a base of white paint. Displacement and strain mapping are then calculated by tracking subsets of the image in the initial state, to a series of images taken during loading. 20 kHz ultrasonic vibration was applied in the study. Transient ultrasonic effect was evaluated with a vibration temporarily applied at the strain of 0.17. The ultrasonic amplitude is 1.3 μm and the strain rate is 0.06/s. Another set of tests was performed where ultrasonic vibration is continuously applied throughout the process. This is to investigate the effects of different test parameters on material flow stress. Two levels of ultrasonic vibration amplitudes, 1.0 μm and 1.3 μm and two levels of strain rate, 0.06/s and 1/s were studied. In situ infrared (IR) thermal imaging was also performed with IR camera mounted over the sample to evaluate the thermal effect of ultrasonic vibration. The evolution of temperature distribution during traditional and ultrasonically assisted (20 kHz, 1.3 μm peak-to-peak amplitude) tensile tests were recorded and compared. Five samples were repeated for each condition mentioned above.

Commercially available electrolytic tough pitch (ETP) copper with a purity of 99.9% in the tempered annealed condition was used in this study. Small scale dogbone specimens shown in Fig. 2 (a) are prepared out of a 0.2 mm copper foil using wire electrical discharge machining (EDM) with the accuracy of 15 μm. To remove potential surface defects during machining, polishing was performed with 1 μm diamond paste prior to testing. Fig. 2 (b) shows the speckle pattern on the specimen. The specimen has a gauge length of 1.7 mm, which is an order of magnitude smaller compared to the wavelength $\lambda = 1/f\sqrt{E/\rho} = 6.13$cm for an ultrasonic sound wave of frequency 20 kHz in copper, where f is the frequency of ultrasonic wave while E and ρ are the elastic modulus

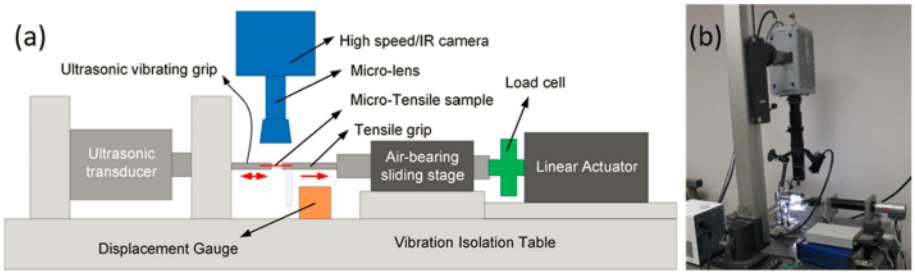

Fig. 1. (a) Schematic illustration of the micro-tensile testbed; (b) Actual experimental setup.

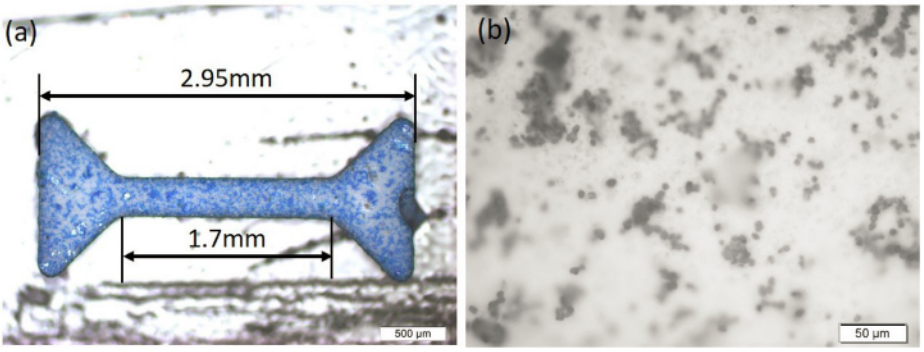

Fig. 2. (a) Small-scale dogbone specimen with speckled pattern; (b) Micro-scale speckles.

and density of copper, respectively.

Microstructure characterizations were performed with optical microscope and EBSD analysis. Mounted copper samples were first grounded with SiC paper to 1200 grid finish, followed by polishing using 3 μm and 1 μm diamond pastes. Final polishing was performed using 0.02 μm colloidal silica. Optical images were taken with Olympus DP2-BSW after etching with a solution of 20 ml distilled water, 20 ml NH_4OH and 5 ml of 3% hydrogen peroxide. EBSD scans were performed on FEI Apreo field emission scanning electron microscope equipped with EDAX Hikari EBSD detector at 20 mm working distance, 13 nA beam current, and 20 kV accelerating voltage. The sample was tilted 70° to horizontal axis and a step size of 0.5 μm was used for all the scans.

3. Results

3.1. The effect of ultrasonic vibration on flow stress

Fig. 3 compares the engineering stress-strain curves obtained from conventional tensile test with no ultrasonic vibration (UA) and the test when UA is temporarily applied for a short period of time during plastic deformation. There is an immediate flow stress drop of around 20 MPa when the ultrasonic vibration is initiated at the strain of 0.17. The amount of flow stress reduction remains approximately unchanged until ultrasonic vibration is turned off, where the flow stress increases instantly. The stress then gradually decreases down to a level that is lower than that without ultrasonic treatment, indicating residual softening occurs.

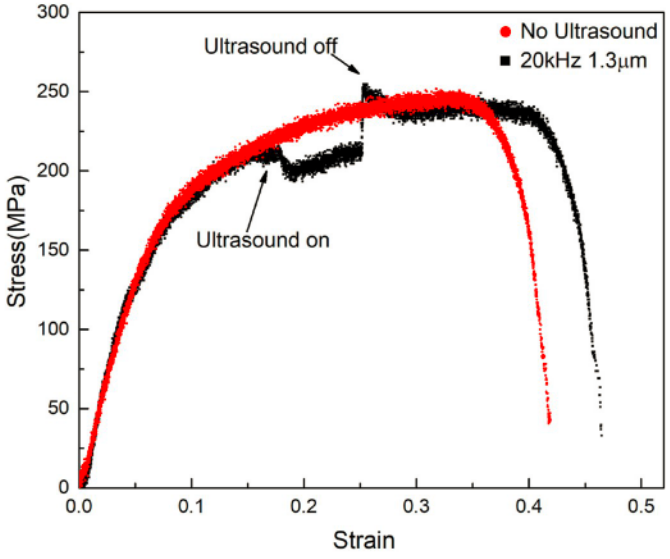

Fig. 3. Engineering stress-strain curves from conventional tension test and the test where UA is temporarily applied at the strain of 0.17 (strain rate: 0.06/s).

Effects of ultrasonic vibration amplitude on the reduction of flow stress are shown in Fig. 4 (a), where the engineering stress-strain curves with no ultrasonic vibration, as well as those with amplitude of 1.0 μm and 1.3 μm are compared. During the initial elastic regime of deformation, where stress changes linearly with strain, little difference is observed between the results of regular and ultrasonically assisted tests. This is attributed to the fact that ultrasonic vibration does not alter the nature of the bonds between atoms. In the plastic deformation regime where the applied stress exceeds yield point of copper, which is around 75 MPa, ultrasonically induced flow stress reduction is consistently observed. With a higher vibration amplitude of 1.3 μm, the flow stress is reduced with a larger amount. Fig. 4 (b) provides a more quantitative comparison of flow stress reduction at different strains and vibration amplitudes with standard deviation. The maximum reduction for 1.0 μm and 1.3 μm is 15.1 MPa and 21.2 MPa, respectively. It can also be observed that the amount of reduction in flow stress increases with increasing strain. This trend holds below a certain strain level and becomes insignificant after 0.2 strain, which is potentially due to the local deformation instabilities and development of necking.

Dependency of ultrasonic softening on strain rate is shown in Fig. 5 (a), where the ultrasonic vibration amplitude is 1.3 μm. Strain rate hardening effect can be noticed for both conventional and ultrasonically assisted tests as it is increased from 0.06/s to 1/s. While ultrasonic softening is observed at both strain rates, there is no statistically significant difference in the amount of flow stress reduction. A more quantitative comparison is provided in Fig. 5 (b), where the flow stress reduction extracted at different levels of strain is plotted with standard deviation. At the two tested strain rates, the amount of flow stress reduction varies in the range of 16–21 MPa and difference between the two strain rates is indistinguishable.

3.2. Digital image correlation (DIC) analysis

Fig. 6 shows the full-field true E_{xx} strain maps for samples tested with and without ultrasonic vibration extracted at 0.1 and 0.2 engineering strain. A significant difference in strain distribution can be noticed with the superimposed ultrasonic vibration. During conventional tensile tests, as shown in Fig. 6 (a) and (b), strain is uniformly distributed with 45-degree shear bands clearly visible and equally spaced along sample gauge. As a comparison, a nonuniform strain distribution is observed under the influence of ultrasonic vibration, as shown in Fig. 6 (c) and (d). The deformation is highly concentrated at one end of the gauge section which is directly connected to the ultrasonic transducer. Shear bands are hardly visible. This localized strain is different from necking phenomenon, which occurs at a later stage of around 0.35 engineering strain due to local deformation instabilities. Neither is it caused by a drastic change in vibration amplitude, as analyzed in the previous experimental session since the length of the small-scale dogbone is one order of magnitude smaller than the ultrasonic wavelength in pure

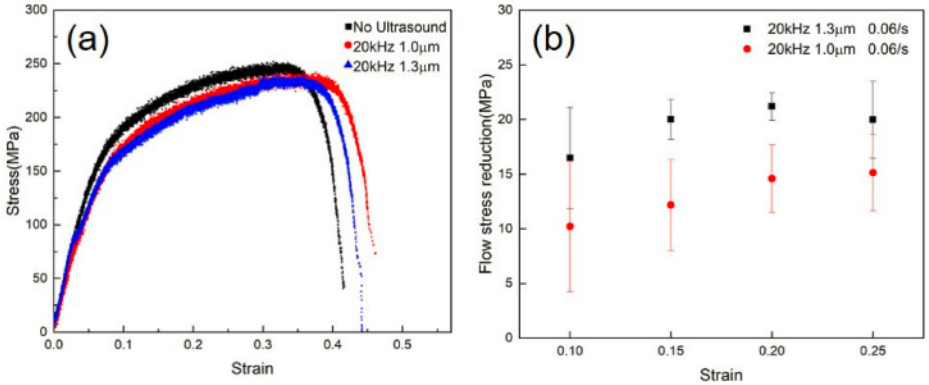

Fig. 4. (a) Engineering stress-strain curves with different ultrasonic vibration amplitudes (Strain rate: 0.06/s); (b) Reduction of flow stress measured at different strains from (a).

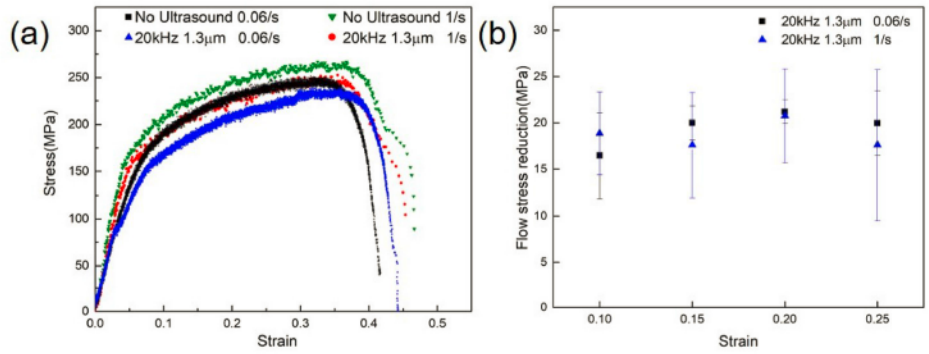

Fig. 5. (a) Engineering stress-strain curves at different strain rates (Ultrasonic amplitude: 1.3 μm); (b) Reduction of flow stress measured at different strains from (a).

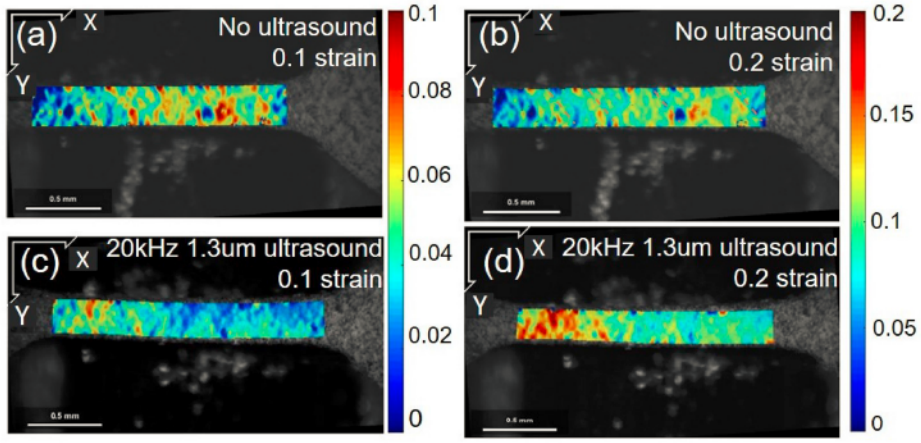

Figure 6. (a–b) DIC results during conventional tensile test at (a) 0.1 and (b) 0.2 engineering strain; (c–d) DIC results during ultrasonically assisted tensile test at (c) 0.1 and (d) 0.2 engineering strain, ultrasonic amplitude is 1.3 μm and strain rate is 0.06/s.

copper. One hypothesis is that the intensity of acoustic energy decays along the specimen length as it is gradually absorbed by the material during propagation. Accordingly, the degree of softening is higher near the ultrasonic transducer side, which corresponds to the higher strain distribution.

3.3. *In situ infrared imaging*

Temperature distribution from infrared (IR) imaging are presented in Fig. 7. Fig. 7 (a) shows the entire field of view from the IR camera and the location of the dogbone specimen which is marked within the dashed line region. The ultrasonic grip is on the left and the moving grip connected to the motor is on the right. Snapshots of thermal images of the tensile test without UA (Fig. 7 (b–d)) and with UA (Fig. 7 (e–g)) are shown in chronological order. In both specimens, a temperature rise is observed during tensile test, noticeably in the gauge section due to plastic deformation. Then temperature goes down as heat dissipates through conduction and convection.

Quantitative analysis is done by comparing the maximum temperature in the region of interest (ROI) which is indicated by the red box in Fig. 7 (a). The rise of maximum temperature ΔT_{max} for tests without and with UA is shown in Fig. 8. Samples tested traditionally experience an

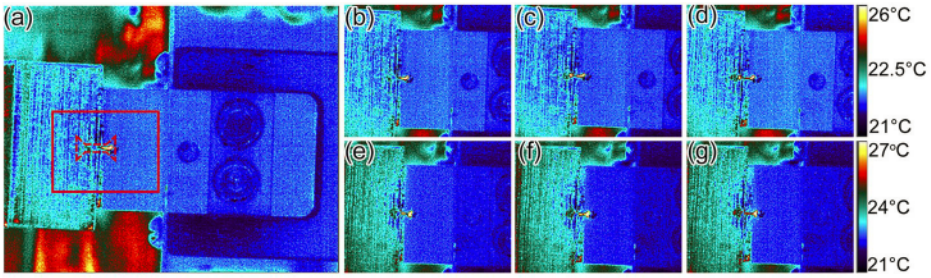

Fig. 7. (a) Field of view of infrared imaging; zoomed in images of tests without UA (b–d) and with UA (e–g) in chronological order, respectively.

average ΔT_{max} of 0.69 °C. With the addition of ultrasonic vibration, the average ΔT_{max} is 1.55 °C, possibly because of the high frequency friction between ultrasonic grip and sample. Overall, the temperature increase is relatively insignificant for thermal softening or inducing microstructure change.

3.4. Microstructural characterization

Fig. 9 shows the optical images for specimens at 0.2 strain with and without UA tested at a strain rate of 0.06/s and the vibration amplitude is 1.3 μm. Distinguished difference in the number of annealing twins can be identified between these two images. Quantitative imaging measurement is performed with the particle analysis function in the ImageJ software. Results show that the area fraction of twinned region is approximately 3.3% without ultrasonic vibration whereas only 1.8% with ultrasonic vibration, which is reduced by 45%.

EBSD results for tensile samples with and without UA are provided in Fig. 10. Fig. 10 (a) and (d) compare the image quality (IQ) maps, where darker color indicates higher lattice distortion, from which high- and low-angle boundaries are identified. In traditional tensile samples (Fig. 10 a), low-angle boundaries occupy a large fraction as a result of dislocation rearrangements to partly release the stored strain energy in plastic deformation. In comparison, the amount of low-angle boundaries is reduced in the ultrasonically tested conditions (Fig. 10 d) even though both samples underwent the same amount of deformation. Table 1 compares the length of low- and high-angle grain boundaries. While the difference of high-angle grain boundary is indistinguishable, the length of low-angle grain boundaries is reduced considerably in the ultrasonically assisted tensile test specimen. For boundaries with misorientation angle between 1° and 5°, the length is reduced to 6.11 cm, which is 45% lower than that without UA.

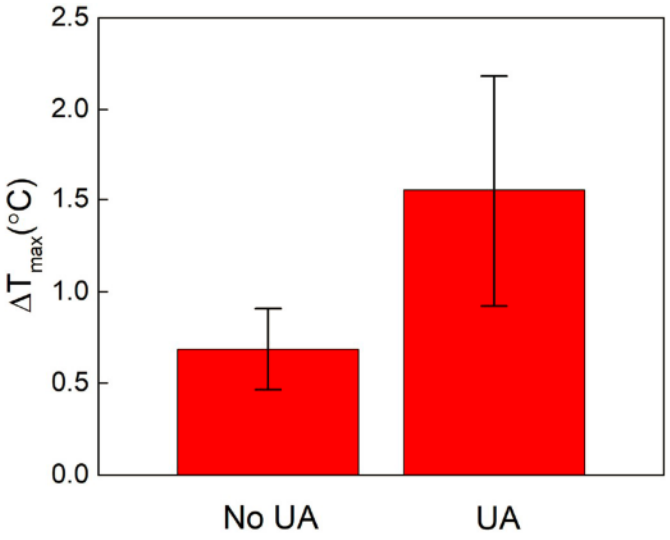

Fig. 8. Comparison of increase in maximum temperature ΔT_{max} in the tensile sample without and with UA.

During plastic deformation, two types of dislocations will be generated, namely statistically stored dislocations (SSD) and geometrically necessary dislocations (GND). The latter one has a nonzero net Burgers vector and is directly associated with local change in crystalline orientation. One common representation of orientation change is the kernel average misorientation (KAM), which is calculated as the average misorientation for a given point with regard to all its neighbors [24]. The KAM map here shows the distribution of misorientation in the range of 0–5°. The 1st nearest neighbor points are used in the calculation. Fig. 10 (b) and (e) compare the KAM values. Higher values across the scan are observed in traditionally tested specimen, with an average angle of 1.24° in Fig. 10 (b). After application of ultrasonic vibration, KAM is reduced to 0.84° with the majority of hot spots concentrated along grain boundaries. The density of GND are then calculated based on the measured misorientation values. GND density map are shown in Fig. 10 (c) and (f). In the conventionally tested specimen, high values of ρ_{gnd} is observed with an average value of $1.24 \times 10^{14} m^{-2}$, which correlate with the high concentration of the low-angle grain boundaries in Fig. 10 (c). As a comparison, the ρ_{gnd} is substantially reduced to an average value of $0.79 \times 10^{14} m^{-2}$ in the ultrasonically assisted tensile specimen (Fig. 10 f), indicating smaller internal strain gradients and more uniform deformation in the microscopic scale.

The evolution of deformation texture is also found to be affected by the applied ultrasonic vibration. Fig. 11 (a), (b) and (c) show the inverse pole figure of rolling direction for samples in the undeformed state, 20% strain and 20% strain with ultrasonic vibration, respectively. The tensile direction during the test aligned with the rolling direction. As illustrated in Fig. 11 (a), the texture of the samples before tensile test is relatively weak. After deformation, a mixture of <001> and <111> texture is observed, which becomes more prominent with the superimposed ultrasonic vibration, especially for <111> direction.

4. Discussion

4.1. The dependence of flow stress reduction on process parameter

In the model proposed by Yao et al. [25] and Saeed Bagherzadeh and Karen Abrinia [19] based on thermal activation of dislocation gliding, the reduction in flow stress is expressed as

$$\Delta\sigma = \sigma_U - \sigma_0 = -\beta\left(\frac{U_E}{\hat{\tau}}\right)^{0.5}$$

where σ_U and σ_0 denote the flow stress with and without UA, the negative sign indicates a stress reduction, β is a material parameter, $\hat{\tau}$ is the mechanical threshold, which is a material property representing the shear strength of a metal at absolute zero temperature. U_E is the acoustic energy density and can be expressed as

$$U_E = \frac{1}{2}\rho\omega^2 A^2$$

where ρ is the density of material, ω and A are angular frequency and

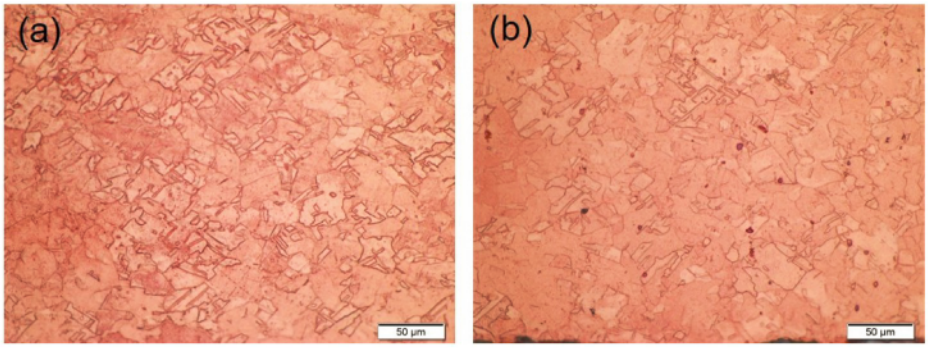

Fig. 9. Optical images of specimen tested with (a) no ultrasonic vibration; (b) 20 kHz 1.3 μm ultrasonic vibration (strain: 0.2, strain rate: 0.06/s).

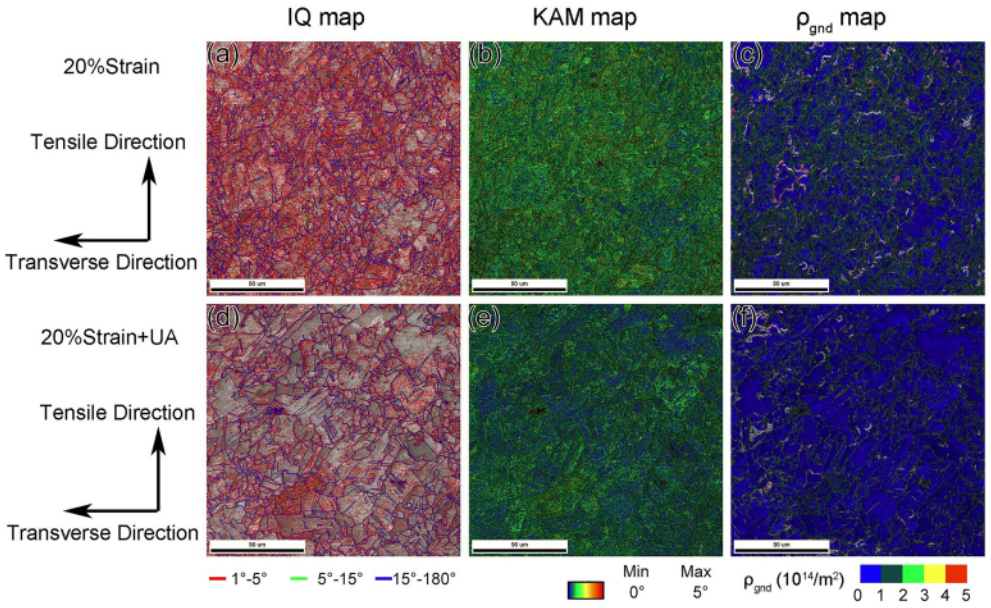

Fig. 10. EBSD results; (a), (b), (c) are image quality (IQ) map, kernel average misorientation (KAM) map and geometrically necessary dislocation (GND) density map without UA, respectively; (b), (d), (f) are the corresponding results with UA.

Table 1
Length of low- and high-angle grain boundaries with and without UA (cm).

	Rotation angle 1°–5°	Rotation angle 5°–15°	Rotation angle 15°–180°
No UA	10.96	0.35	2.75
UA	6.11	0.07	2.37

amplitude of the ultrasonic wave, respectively. Combining these two equations, the flow stress reduction is found to be proportional to the applied ultrasonic vibration amplitude. By plotting the experimentally measured stress reduction at 0.1 strain at different amplitude in Fig. 12, a linear relationship is observed, which agrees with the theoretical prediction.

The difference in flow stress reduction under the two tested strain rates (0.06/s and 1/s) is indistinguishable. Similar results were reported by Prabhakar et al. [26], where they found the reduction of flow stress is insensitive to strain rate in the range of 1.04×10^{-4}-1.04×10^{-2}/s for aluminum alloy AA 6063. On the other hand, the model proposed by Sedaghat et al. [14] suggested the dependence of flow stress reduction on strain rate. This is potentially because studied range of strain rate in the experiment is relatively small to reveal its effects.

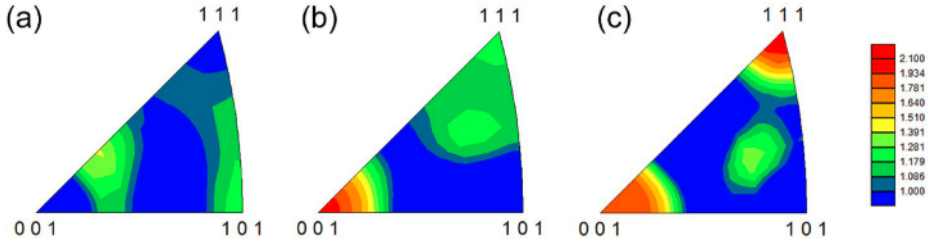

Fig. 11. Inverse pole figure of tensile direction of (a) undeformed sample; (b) 20% strain; (c) 20% strain with UA.

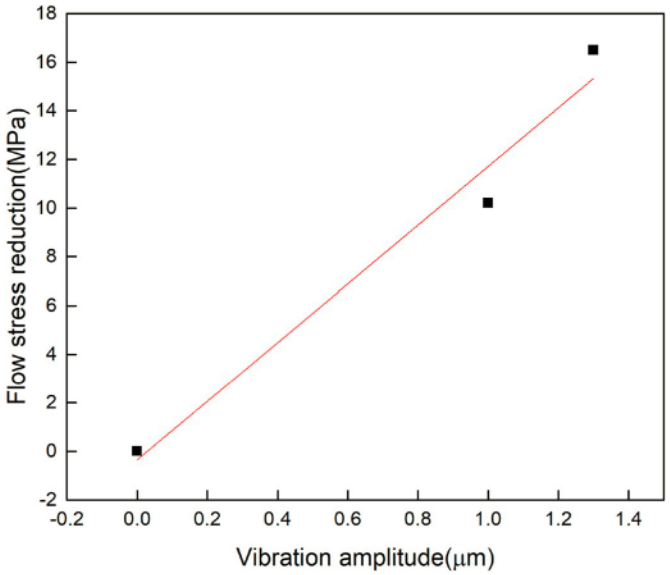

Fig. 12. Relationship of flow stress reduction with regard to vibration amplitudes (strain: 0.1, strain rate: 0.06/s).

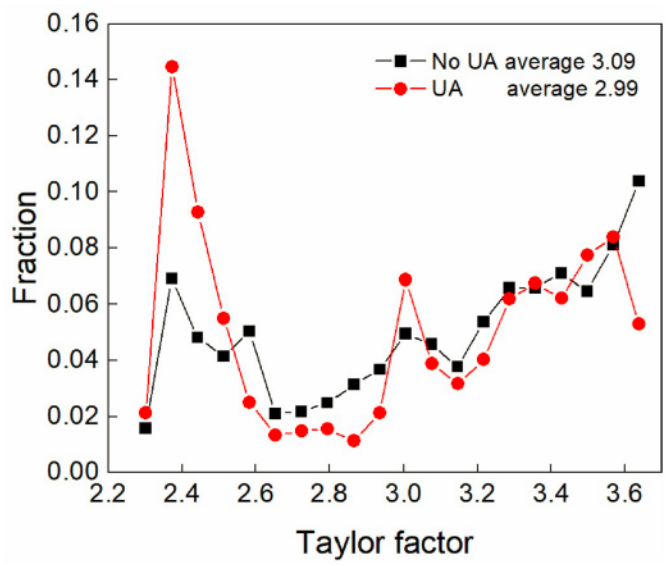

Fig. 13. Distribution of Taylor factor for tensile samples with and without UA.

4.2. Microstructural change and residual softening mechanism

Optical microscopy and EBSD reveals a significant reduction in the area fraction of twinning. For FCC metals subjected to cold-working and subsequent annealing treatment, annealing twins with the straight-sided lamella morphology are formed because of their relatively lower stacking fault energy. Field et al. [27] reported migration of twin boundary in annealed copper during plastic deformation, where narrow twins separated by parallel boundaries completely disappear through the process that boundary on one side migrates and annihilates with the other one. It was explained that the twin boundaries act as non-regenerative sources for dislocations, where a $1/3(\overline{111})$ dislocation on the twin boundary step is dissociated into a Shockley partial $1/6(\overline{211})$ and a stair-rod dislocation $1/6(0\overline{11})$. The $1/3(\overline{111})$ dislocation on twin boundary step can also interact with a Shockley partial dislocation, resulting in a $1/2(110)$ perfect dislocation. This accordingly allows the twin boundaries to migrate as deformation proceeds. In this study, the migration and annihilation of annealing twin boundary is enhanced with the application of ultrasonic vibration. This could be attributed to lower activation energy for dislocation dissociation with additional ultrasonic energy and improved dislocation mobility.

It is shown from the thermal imaging that the temperature rise associated with ultrasonic vibration is around 1.55 °C and accordingly contributes only a minor portion of the reduction of flow stress observed in the ultrasonically assisted tensile tests. In situ ultrasonic vibration can induce intrinsic material microstructure change as shown in EBSD results, which is also reflected as the residual softening effect on the stress-strain curve in the intermittent test (Fig. 3). For FCC polycrystals, a mixture of <111> and <001> texture will develop after uniaxial tension and the texture will be more significant under higher amount of deformation [28,29]. With the applied ultrasonic vibration, development of these textures can be enhanced. As shown in Fig. 11 (b) and (c), for the same amount of deformation, higher intensity on <111> is observed in the ultrasonically tested sample. This also indicates that lattice rotation is facilitated with ultrasonic vibration. Fig. 13 compares the distribution of Taylor factor and the fraction of low-value Taylor factor is considerably higher in the ultrasonically tested sample. The average Taylor factor is 2.99, which is lower than the average value 3.09 in the traditionally tested specimen. Zhou et al. also observed similar phenomena on grain orientation change and reduction of Taylor factor when they did ultrasonic assisted compression on aluminum [11]. This indicates that ultrasonic vibration promotes lattice rotation towards the easier slip condition, which correspond to the drop in flow stress. A possible explanation regarding this ultrasonic effect can be considered as followings: Deformation of the material is achieved with both lattice stretch and reorientation [30]. The amplitude of ultrasonic vibration for UA material deformation tests in the current literature varies from 1 μm to 100 μm, which is generally in the same range as the grain size. Under the simultaneously applied load, certain amount of vibration displacement can be accommodated by lattice rotation. As the grain orientation sweeps from the minimum to the maximum angle during the vibration cycle, at certain stage, the grain is reoriented in a desired angle where the resolved shear stress on the activated slip system is greatly increased and additional slip systems are triggered, which accordingly promotes deformation. This is similar to geometric softening of crystal [26], but facilitated with the ultrasonic vibration.

Low-angle grain boundary is a dislocation structure that forms as a result of dislocation regrouping to partially release stored strain energy due to plastic deformation [9]. Regions with concentrated low-angle grain boundary indicate areas of high GND density [24]. With ultrasonic vibration, ρ_{gnd} is significantly reduced and is mostly observed in the vicinity of grain boundaries. This could be attributed to the increased dislocation mobility with ultrasonic vibration, which increases the probability of dislocation annihilation [9]. In addition, less amount of dislocation pileup is generated with easier slip condition. The results in this study are different from the observations of Siu et al. [10], where ultrasonic vibration showed to promote subgrain formation for FCC aluminum. This is related to the relative direction of movement between ultrasonic vibration and material deformation. In the experimental configuration of Siu et al. [10], the vibration is transverse to the compression direction, which introduces additional shear stress. In this study with micro-tensile tests, the vibration is longitudinal along the tension direction and only normal stress is involved in the continuum scale.

The modified microstructure features, including reduced amount of annealing twin boundary, reoriented grains and less internal misorientation can all contribute to the residual softening observed in the tensile stress-strain curve, since these are all permanent effects on the material microstructure generated by ultrasonic vibration.

5. Conclusion

Micro-tensile test of pure copper was conducted to investigate the

effect of simultaneous ultrasonic vibration during plastic deformation. When 20 kHz 1.3 μm ultrasonic vibration is temporarily applied, the material flow stress immediately dropped with around 20 MPa and residual softening is observed after ultrasonic vibration is stopped. Effects of vibration amplitude and strain rate were studied with continuous ultrasonic vibration throughout the tests. It is found that the flow stress reduction is more significant when vibration amplitude increases from 1.0 μm to 1.3 μm, which agrees with a linear relationship reported in literature. Change in flow stress reduction is insignificant when strain rate increases from 0.06/s to 1/s. In situ DIC analysis shows that with the superimposed ultrasonic vibration, strain localizes in the gauge section near ultrasonic source whereas uniform strain distribution was observed in conventional tensile tests. Optical microstructure characterization shows a reduction in the fraction of annealing twins in the ultrasonically assisted specimens. Infrared imaging shows that the temperature rise associated with ultrasonic vibration is minimal. From EBSD analysis, it is revealed that ultrasonic vibrations promote preferential grain reorientation and reduces the internal misorientation within grains.

Declaration of competing interest

The authors declare that they have no known competing financial interests or personal relationships that could have appeared to influence the work reported in this paper.

CRediT authorship contribution statement

Jiarui Kang: Conceptualization, Methodology, Validation, Investigation, Formal analysis, Visualization, Writing - original draft. **Xun Liu:** Conceptualization, Methodology, Formal analysis, Supervision, Writing - review & editing. **Mingjie Xu:** Investigation, Formal analysis.

Acknowledgement

This work was supported by National Science Foundation under the grant No. 1841589. The authors express thanks to Dr. Michael Mills and Dr. Avraham Benatar for support in experimental equipment and Dr. Elvin Beach for suggestions on sample preparation. The authors would also like to acknowledge the EBSD characterization facilities provided by the University of California, Irvine Materials Research Institute (IMRI) and the Center for Electron Microscopy and Analysis (CEMAS) at The Ohio State University.

References

[1] F. Blaha, B. Langenecker, Tensile deformation of zinc crystal under ultrasonic vibration, Naturwissenschaften 42 (1955) 1–10.
[2] K.F. Graff, Ultrasonic Metal Forming: Materials, in: J.A. Gallego-Juárez, K.F. Graff (Eds.), Power Ultrasonics, Woodhead Publishing, Oxford, 2015, pp. 337–376, https://doi.org/10.1016/B978-1-78242-028-6.00014-4.
[3] B. Langenecker, Effects of ultrasound on deformation characteristics of metals, IEEE Trans. Son. Ultrason. 13 (1966) 1–8, https://doi.org/10.1109/T-SU.1966.29367.
[4] K. Siegert, J. Ulmer, Superimposing ultrasonic waves on the dies in tube and wire drawing, J. Eng. Mater. Technol. Trans. ASME. 123 (2001) 517–523, https://doi.org/10.1115/1.1397779.
[5] C. Bunget, G. Ngaile, Influence of ultrasonic vibration on micro-extrusion, Ultrasonics 51 (2011) 606–616, https://doi.org/10.1016/j.ultras.2011.01.001.
[6] R. Cheng, N. Wiley, M. Short, X. Liu, A. Taub, Applying ultrasonic vibration during single-point and two-point incremental sheet forming, Procedia Manuf 34 (2019) 186–192, https://doi.org/10.1016/j.promfg.2019.06.137.
[7] G.E. Nevill, Effect of vibrations on the yield strength of a low carbon steel, Rice University, https://hdl.handle.net/1911/89167, 1957.
[8] Y. Daud, M. Lucas, Z. Huang, Modelling the effects of superimposed ultrasonic vibrations on tension and compression tests of aluminium, J. Mater. Process. Technol. 186 (2007) 179–190, https://doi.org/10.1016/j.jmatprotec.2006.12.032.
[9] R.K. Dutta, R.H. Petrov, R. Delhez, M.J.M. Hermans, I.M. Richardson, A.J. Böttger, The effect of tensile deformation by in situ ultrasonic treatment on the microstructure of low-carbon steel, Acta Mater. 61 (2013) 1592–1602, https://doi.org/10.1016/j.actamat.2012.11.036.
[10] K.W. Siu, A.H.W. Ngan, I.P. Jones, New insight on acoustoplasticity - ultrasonic irradiation enhances subgrain formation during deformation, Int. J. Plast. 27 (2011) 788–800, https://doi.org/10.1016/j.ijplas.2010.09.007.
[11] H. Zhou, H. Cui, Q.H. Qin, Influence of ultrasonic vibration on the plasticity of metals during compression process, J. Mater. Process. Technol. 251 (2018) 146–159, https://doi.org/10.1016/j.jmatprotec.2017.08.021.
[12] T. Liu, J. Lin, Y. Guan, Z. Xie, L. Zhu, J. Zhai, Effects of ultrasonic vibration on the compression of pure titanium, Ultrasonics 89 (2018) 26–33, https://doi.org/10.1016/j.ultras.2018.04.006.
[13] A. Siddiq, T. El Sayed, Acoustic softening in metals during ultrasonic assisted deformation via CP-FEM, Mater. Lett. 65 (2011) 356–359, https://doi.org/10.1016/j.matlet.2010.10.031.
[14] H. Sedaghat, W. Xu, L. Zhang, Ultrasonic vibration-assisted metal forming: constitutive modelling of acoustoplasticity and applications, J. Mater. Process. Technol. 265 (2019) 122–129, https://doi.org/10.1016/j.jmatprotec.2018.10.012.
[15] A. Deshpande, K. Hsu, Acoustic energy enabled dynamic recovery in aluminium and its effects on stress evolution and post-deformation microstructure, Mater. Sci. Eng. 711 (2018) 62–68, https://doi.org/10.1016/j.msea.2017.11.015.
[16] Z. Xie, Y. Guan, X. Yu, L. Zhu, J. Lin, Effects of ultrasonic vibration on performance and microstructure of AZ31 magnesium alloy under tensile deformation, J. Cent. South Univ. 25 (2018) 1545–1559, https://doi.org/10.1007/s11771-018-3847-z.
[17] V. Fartashvand, A. Abdullah, S.A. Sadough Vanini, Investigation of Ti-6Al-4V alloy acoustic softening, Ultrason. Sonochem. 38 (2017) 744–749, https://doi.org/10.1016/j.ultsonch.2016.07.007.
[18] H. Huang, A. Pequegnat, B.H. Chang, M. Mayer, D. Du, Y. Zhou, Influence of superimposed ultrasound on deformability of Cu, J. Appl. Phys. 106 (2009) 113514, https://doi.org/10.1063/1.3266170.
[19] S. Bagherzadeh, K. Abrinia, Effect of ultrasonic vibration on compression behavior and microstructural characteristics of commercially pure aluminum, J. Mater. Eng. Perform. 24 (2015) 4364–4376, https://doi.org/10.1007/s11665-015-1730-8.
[20] J. Hu, T. Shimizu, M. Yang, Investigation on ultrasonic volume effects: stress superposition, acoustic softening and dynamic impact, Ultrason. Sonochem. 48 (2018) 240–248, https://doi.org/10.1016/j.ultsonch.2018.05.039.
[21] J.C. Hung, C.C. Lin, Investigations on the material property changes of ultrasonic-vibration assisted aluminum alloy upsetting, Mater. Des. 45 (2013) 412–420, https://doi.org/10.1016/j.matdes.2012.07.021.
[22] K. May, Small Scale Tensile Testing of Titanium Alloys, The Ohio State University, 2010.
[23] J. Blaber, B. Adair, A. Antoniou, Ncorr: open-source 2D digital image correlation matlab software, Exp. Mech. 55 (2015) 1105–1122, https://doi.org/10.1007/s11340-015-0009-1.
[24] S.I. Wright, M.M. Nowell, D.P. Field, A review of strain analysis using electron backscatter diffraction, Microsc. Microanal. 17 (2011) 316–329, https://doi.org/10.1017/S1431927611000055.
[25] Z. Yao, G.Y. Kim, Z. Wang, L.A. Faidley, Q. Zou, D. Mei, Z. Chen, Acoustic softening and residual hardening in aluminum: modeling and experiments, Int. J. Plast. 39 (2012) 75–87, https://doi.org/10.1016/j.ijplas.2012.06.003.
[26] A. Prabhakar, G.C. Verma, K. Hariharan, P.M. Pandey, M.G. Lee, S. Suwas, Dislocation density based constitutive model for ultrasonic assisted deformation, Mech. Res. Commun. 85 (2017) 76–80, https://doi.org/10.1016/j.mechrescom.2017.08.003.
[27] D.P. Field, B.W. True, T.M. Lillo, J.E. Flinn, Observation of twin boundary migration in copper during deformation, Mater. Sci. Eng. 372 (2004) 173–179, https://doi.org/10.1016/j.msea.2003.12.044.
[28] G. Lin, K.S. Havner, On the evolution of texture and yield loci in axisymmetric deformation of F.C.C. polycrystals, Int. J. Plast. 10 (1994) 471–498, https://doi.org/10.1016/0749-6419(94)90010-8.
[29] S. Ahzi, S. M'Guil, Simulation of deformation texture evolution using an intermediate model, Solid State Phenom. 105 (2005) 251–258. www.scientific.net/ssp.105.251.
[30] R.J. Asaro, Crystal plasticity, J. Appl. Mech. 50 (1983) 921–934, https://doi.org/10.1115/1.3167205.